Journal of Cleaner Production 148 (2017) 958–968

Contents lists available at ScienceDirect

Journal of Cleaner Production

journal homepage: www.elsevier.com/locate/jclepro

Equilibrium, kinetic, and thermodynamic studies of lead ion and zinc ion adsorption from aqueous solution onto activated carbon prepared from palm oil mill effluent

Ganiyu Abimbola Adebisi [a], Zaira Zaman Chowdhury [a, **], Peter Adeniyi Alaba [b, *]

[a] Nanotechnology & Catalysis Research centre (NANOCAT), University of Malaya, IPS Building, 50603 Kuala Lumpur, Malaysia
[b] Department of Chemical Engineering, University of Malaya, 50603 Kuala Lumpur, Malaysia

ARTICLE INFO

Article history:
Received 19 November 2016
Received in revised form
6 February 2017
Accepted 6 February 2017
Available online 8 February 2017

Keywords:
Activated carbon
Adsorption
POME
Equilibrium
Isotherm
Thermodynamic

ABSTRACT

An efficient activated carbon was prepared using palm oil mill effluent as a precursor. The adsorption capacity of activated carbon for lead ion and zinc ion from aqueous media was investigated under equilibrium conditions between 303.15 and 353.15 K. The activated carbon was analyzed using fourier transform infrared spectroscopy, field emission scanning electron microscope, energy dispersive X-Ray, and Nitrogen adsorption-desorption analysis. The adsorption capacity of activated carbon was studied by varying adsorbent dosage, contact time, and temperature. The equilibrium time was attained after 50 min for both ions. The data analysis was performed with different isotherm and kinetic models. Pseudo-second-order kinetic rather than pseudo first-order model is best fitted for both lead ion and zinc ion removal from wastewater. Further, the rate-determining step for both metal ions is chemisorption based on the suitability of the Elovich equation. Langmuir model provides the best fit for both removal of lead ion and zinc ion. The thermodynamic parameters shows the feasibility of adsorption of both ions is endothermic.

1. Introduction

Heavy metals are discharged into water bodies through various industrial activities especially in the manufacturing and mining industries. They are highly toxic and usually constitute health hazards when consumed beyond the permissible and bearable amount. Heavy metal pollutants have been removed from wastewaters using various technologies ranging from precipitation, reverse osmosis, membrane filtration and ion exchange (Baccar et al., 2009). However, these technologies have several disadvantages such as requirement of expensive equipment and the need of chemicals, which may in turn pollute the water. Due to these limitations, there is vital need for a more environmentally benign and cost effective method. Several efforts were geared towards the use of adsorption process. The use of adsorbents in heavy metal removal from wastewaters has not only been found to be superior to other conventional methods, but it has equally been found to be cost-effective, simple in design, easy to operate and much more environmentally benign (Naje et al., 2016). In view of this, substantial attention has been given to development of cheap adsorbents such as kaolin (Alaba et al., 2016a), bentonite, fly ash blast furnace slag and activated carbon for removal of the different heavy metals at low concentration (Mishra and Patel, 2009).

Palm oil is one of the most significant vegetable oils globally with Malaysia being the largest producer and exporter (Sani et al., 2015). During palm oil processing, several products and by-products generated include palm oil, palm kernel, palm oil mill effluent (POME), shell, empty fruit bunch (EFB) and fiber (Sani et al., 2015). The palm oil mill industry is said to be the major source of industrial pollution in Malaysia (Phang, 1990). They discharges more than 15million ton of POME from more than 110 processing mill (Board, 2003) into the environment, thereby constituting a serious environmental pollution especially in the waterways (Phang and Kim-Chong, 1988). The discharge of POME, either untreated or poorly treated, into the environment can lead to serious hazards ranging from pollution of groundwater, release of methane into the atmosphere to release of unpleasant odor to the environment (Chavalparit, 2006). Several methods have been adopted to treat POME before the discharge including sedimentation, filtration

* Corresponding author.
** Corresponding author.
E-mail addresses: adebisi@siswa.um.edu.my (G.A. Adebisi), dr.zaira.chowdhury@um.edu.my (Z.Z. Chowdhury), adeniyipee@live.com (P.A. Alaba).

http://dx.doi.org/10.1016/j.jclepro.2017.02.047
0959-6526/

and decolourization (Igwe and Onyegbado, 2007). Other techniques involve ion exchange, adsorption, reverse osmosis, selective crystallization, and coagulation processes. Interestingly, POME has been reported to be rich in protein, nitrogenous compounds, carbohydrate, lipids and minerals (Habib et al., 1997). POME equally contains lignocellulosic wastes as well as mixture of oil and carbohydrates (Oswal et al., 2002). This makes this renewable, readily available and abundant agricultural waste a viable alternative precursor for activated carbon synthesis. Activated carbons have been in use as adsorbents for quite a while. Nonetheless, the commercial activated carbons are relatively expensive; hence, the need for utilization of lignocellulosic wastes for the synthesis of activated carbons (Nacu et al., 2015). A few of the agricultural wastes that have been used as a precursor for synthesis of activated carbon adsorbents include solid wastes (Alaba et al., 2015), coconut shell (Amuda et al., 2007), kenaf core (Chowdhury et al., 2012a), bamboo culms (Ekebafe et al., 2012), oil palm empty fruit bunch (Foo and Hameed, 2011), coconut shell (Gratuito et al., 2008), rattan sawdust (Hameed et al., 2007) and a host of others. However, the quality (characteristics) and quantity (yield) of activated carbon that can be produced from a particular raw material depend on two main factors, that is, the nature of the precursor itself and the successful manipulation of the process conditions as it will require an optimum conditions to obtain the required characteristics of the activated carbon (Gratuito et al., 2008). Considering the nature of the precursor, a precursor with high cellulose content will lead to production of a microporous activated carbon, while one with a high lignin content will give activated carbon that will be highly mesoporous. To obtain a balanced process conditions will require strict monitoring of such variables as carbonization temperature, holding time and chemical impregnation ratio.

This study is aimed to evaluate the efficiency of POME activated carbon (POMEAC) for removal of Pb (II) and Zn (II) ions from wastewater for the first time. The material was characterized using various microscopic and spectroscopic examinations and its performance was evaluated for Pb (II) and Zn (II) uptake from wastewater. The experimental variables of influence on the sorption experiment like contact time, temperature and initial metal ions concentration were investigated. The analysis of equilibrium adsorption of the experimental data was performed by kinetic models, and various isotherms. The thermodynamic variables (ΔH°, ΔS° and ΔG°) for sorption experiments were also determined.

2. Methodology

2.1. Collection and treatment of palm oil mill effluent (POME) sample

The POME sludge was obtained from a local palm oil mill plant in Osogbo, Osun state, Nigeria. The point of collection was situated at a site before the discharge of the POME into the treatment pond. After collection, the sample was thoroughly filtered with distilled water to eliminate dirt such as mud and other impurities. Further, the sample was sun-dried in a wide-mouthed plastic container for 2 months after which it was preserved in a desiccator to avoid possible bio-degradation. Further, the sample was filtered with distil-water, and dried in oven at 60 °C for 24 h. The resulting samples were pulverized to <1 μm mesh size with the aid of a jaw crusher (Denver Product, Dagenham, U.K).

2.2. Preparation of activated carbon

Towards synthesis of activated carbon, the effects of the different process variables such as holding time, carbonization temperature and H_3PO_4 concentration on the yield and porosity of activated carbon were studied. For each of the variables, the sample was fed into the urns of about 150 mm length and 40 mm diameter. The urns was then transferred into the calcination furnace (Bamstead/Thermolyne 48000) fitted with a temperature knob to regulate the temperature. The urns was equally connected to nitrogen gas cylinder while the sample pyrolysis was carried out using a continuous nitrogen gas flow of 100 mL min^{-1} at varying temperature between 500 and 800 °C. After the regulated holding time, the samples were cooled to room temperature under inert atmosphere, and subsequently raked from the vessel. The sample was then filtered with distilled water to eliminate residual chemical agents until the pH became neutral and then dried at 65 °C for 12 h.

2.2.1. Impregnation of the sample with H_3PO_4

The sample was activated with H_3PO_4 and the influence of H_3PO_4 concentration on the yield and porous characteristics of POMEAC were studied. 20 g of the sample was impregnated with H_3PO_4 in varying impregnation ratio ranging from 30% to 50%.

2.2.2. Carbonization of the impregnated samples

The samples impregnated with H_3PO_4 were carbonized and the influence of carbonization temperature on the porosity and yield of activated carbon during activation process was observed. This was investigated by varying the carbonization temperature from 500 to 800 °C for the chemically activated sample. The holding time was also varied from 1 to 3 h.

2.3. Physico-chemical characteristics of POMEAC

The functional groups and structure of the prepared POMEAC were obtained using the FTIR spectroscopy. The FTIR analysis of both the raw POME and POMEAC were obtained from 400 to 4000 cm^{-1} using FTIR- 2,000, Perkin Elmerc.

The surface morphology of both the raw POME and POMEAC were analyzed with field electron scanning electron microscope (FESEM) (Zeiss SUPRA 35VP; Germany) coupled with energy dispersive x-ray spectrometer for elemental analysis.

2.4. Sorption of Pb (II) and Zn (II) ions on the adsorbent

The sorption of the adsorbates onto the adsorbents was studied through batch adsorption studies. Variation of uptake level of Pb(II) and Zn(II) ions with contact time was determined for each of the adsorbent. This was required in other to establish the equilibrium time (time for the adsorbent to reach sorption equilibrium). To accomplish this, 0.2 g each of the adsorbent were dispersed in 50 cm^3 of each of the initial concentrations of 150, 200, 250, 300 and 350 mg L^{-1} solutions at a time range of 10–360 min in well stoppered plastic containers. The minimum amount of adsorbent was used to examine the possibility of achieving a remarkable adsorption performance by varying other operating parameters. The mixture was then thoroughly agitated using a water bath shaker set at 150 rpm and at room temperature (30 °C). Subsequently, the mixture was filtered and the residual concentration of the Pb(II) and Zn(II) ions (as the case may be) in the filtrate was determined by ICP (APHA 3125B, 20th edition, 1998). The quantity of Pb(II) or Zn(II) removed at equilibrium (qe) was estimated from the following equation.

$$q_e = \frac{(C_o + C_e)V}{W} \quad (1)$$

where,q_e (mg/g) = quantity of adsorbate (Pb(II) or Zn(II) ions) adsorbed at equilibrium, C_o (mg/L) = initial concentration of adsorbate,C_e (mg/L) = final concentration of adsorbate after

adsorption at equilibrium.V (L) = Volume of solution.W (g) = Mass of dry adsorbent.

3. Results and discussion

3.1. Effects of process variables on the yield of activated carbon

The effects of the process variables on the quality (porous characteristics) and quantity (yield) on activated carbon prepared from a particular precursor cannot be underestimated as the yield and development of porosity depends largely on such variables as carbonization temperature, holding time and impregnation ratio.

3.1.1. Carbonization temperature

Fig. 1a below elucidates the influence of carbonization temperature on the preparation of activated carbon from POME using H_3PO_4 as the activating agent using 25% acid concentration for 2 h. It is evident from the figure that the yield (%) decreased with increase in carbonization temperature. This is as a result of such losses in form of carbon burn-off and other volatiles at higher temperatures (Mi et al., 2015). Increase in temperature from 500 °C to 800 °C leads to decrease in the yield of activated carbon from 43.76% to 25.59%, indicating that the optimum carbonization temperature is 500 °C.

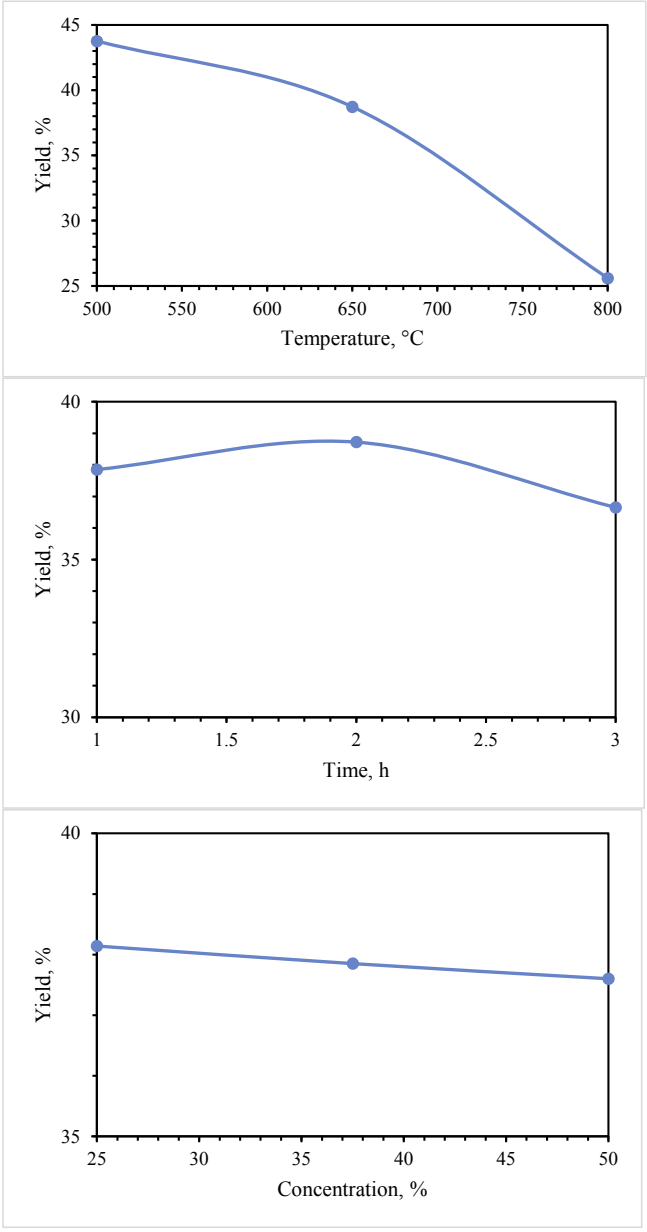

Fig. 1. Effect of (a) carbonization temperature, (b) holding time (c) acid concentration on the yield of POMEAC.

3.1.2. Holding time

In addition to other process variables, the holding time plays important role in determining the yield (%) and porous characteristics of activated carbon prepared from a precursor. In this case, by keeping the carbonization temperature and impregnation ratio constant at 650 °C and 37.50%, the holding time was varied between 1 h–3 h.

Fig. 1b below shows the effect of holding time on the POME activated carbon (PAC) preparation. It could be perceived from the figure that the yield of POMEAC initially increases as the holding time increases from 1 to 2 h, indicating that the optimum holding time is 2 h. However, further increase in the holding time decreases the yield. This is mainly due to the severity of carbon burn-off with increase in holding time. Similar result was observed by (Mi et al., 2015).

3.1.3. Acid concentration

The concentration of the impregnating agent (H_3PO_4) used for the synthesis was varied from 25% to 50%. The yield of carbon from a precursor depends largely on the amount of carbon released to bind with oxygen and hydrogen atoms during transformation from lignocellulosic materials. The conversion from lignocellulosic wastes into carbon usually involves the release of O and H atoms in form of aldehydes, CO_2, CO, CH_4 and H_2O (Tseng, 2007).

Fig. 1c below indicates the effect, which the impregnation ratio as well as the impregnating agent has on the POME activated carbon (PAC) yield (%) at 650 °C for 1 h. From the figure, it is vivid that the yield of POMEAC decreased from 38.14 to 37.60% as the concentration of H_3PO_4 increased from 25% to 50%, indicating that the optimum acid concentration is 25%. This is traceable to severe leaching carbon atoms released in form of CO_2, CO, CH_4 and aldehydes.

3.2. Characterization

3.2.1. Porosity analysis

Pore diameter, pore volume and Surface area of the POME and POMEAC obtained at optimum conditions were determined by using a Micromeritics BET instrument using ultra-pure nitrogen adsorption at −196 °C. Average values of these properties were given in Table 1 below.

Fig. 2 illustrates N_2 adsorption-desorption isotherms (at −196 °C) of POME and POMEAC. Both isotherms are type IV according to the IUPAC classification (Sing, 1985), which is characterized by hysteresis loop. The high N_2 adsorbed amount on POMEAC indicates its high porosity. This is traceable to removal of inorganic and water-soluble organic matters, which opens the pore structure and enhances the porosity (Alaba et al., 2016b).

3.2.2. EDX analysis

The elemental composition of the samples were analyzed using energy dispersive analysis system of X-ray (EDX) (EDX, Ltd., USA). EDX analysis was conducted to evaluate the adsorption of cadmium on CCB beads. The spectrum of POMEAC shows the presence of C, O, Al, Si, K, P, Fe and Ca in the structure (Fig. 3). Table 1 presents the elemental percentage composition of the samples. The effect of

Table 1
Textural properties and elemental composition of POME and POMEAC.

Properties	POME	POMEAC
S_{BET} (m^2/g)	1.8056	59.1989
S_{micro} (m^2/g)	0.3546	38.0977
V_{micro} (cm^3/g)	0.0001	0.0173
V_{total} (cm^3/g)	0.0060	0.0348
D_p (nm)	13.24	2.36
EDX (Weight%)		
C K	68.19	47.07
O K	30.45	38.02
Al K	0.28	0.57
Si K	0.56	1.43
K K	0.25	0.65
Ca K	0.25	0.34
Fe K	0.02	0.03
P K	0	11.89

H_3PO_4 activation on POME is evident by the presence of phosphorus (P) and reduction in the percentage composition of carbon due to carbon burn-off.

3.2.3. FTIR

The FTIR spectra of both the sample (POME) and the prepared POME activated carbon (POMEAC) are shown in Fig. 4 below. The POME spectra show different peaks corresponding to different functional groups. The spectra peaks at 3860.02 and 3433.06 cm^{-1} correspond to –NH associated with amide in bonded form and –OH functional groups of phenol. The peaks at 2923.59 and 2854.71 cm^{-1} designate the presence of –C–H stretching in methyl and methylene groups asymmetric and symmetric stretching. Other functional groups that are present, according to the spectra peaks are the ether groups (R-OR^-) at 1741.53 cm^{-1}, carbonyl groups (C=O) at 1641.12 cm^{-1}, esters group (R-C–O-R^-) at 1382.71 cm^{-1}, –C–O– stretching at 1170.88 cm^{-1} and group –C=O groups at 1027.87 cm^{-1} spectral peak.

The activation of POME to POMEAC leads to decrease in intensities of the above peaks except the peak at 1027.87 cm^{-1}, which increases and shifts to 1037.52 cm^{-1} due to in-plane deformation of aromatic –CH. Other bands above 600, which are ascribed to alkenes and aromatics out of plane bend with acyclic C–O–C groups conjugated with carbon-carbon double bounds (C=C–O–C) in olefinic or aromatic structures. This indicates that POMEAC is rich in basic surface functional group, which are suitable for adsorption of hydrophobic pollutants.

3.2.4. FESEM

The FESEM analysis was performed using software controlled digital FESEM equipment. Fig. 5 presents the result of the micrograph for the raw material and product. The FESEM of POME shows that it is amorphous. Further, the micrograph illustrates the porosity of POMEAC with various sizes of pore openings on the surface, which increase the contact area, and facilitates mass transfer the pore during adsorption.

3.3. Batch adsorption study

From economic point of view, it is essential to study the influence of adsorbent dosage to determine the minimum weight of adsorbent required for effective metal ion removal. Fig. 6 (a) presents the influence of adsorbent dosage on sorption of Pb(II) and Zn(II). It is evident that the removal of both metal ion increases with increase in the quantity of adsorbent used. Moreover, increase in the adsorbent dosage also favors the equilibrium adsorption capacity (mg g^{-1}) (Fig. 6 (b)). However, economic viability of the process is of vital importance. We used 0.2 g to investigate the feasibility of better adsorption performance by varying other parameters. This is in agreement with the submissions of the work of (Lupea et al., 2012).

3.4. Adsorption kinetics

To determine the adsorption equilibrium time for the two pollutants, batch adsorption studies were carried out at varying times ranging from 10 to 360 min, at 30 °C and pH 5.5 as used by Chowdhury et al. (2012b,c). The choice of pH value is also based on the understanding from the study of Chigondo et al. (2013) on the adsorption of Pb(II) and Zn(II) ions onto POMEAC at T = 30 °C, t = 210 min, adsorbate initial concentration = 350 mg L^{-1} and adsorbent dosage = 0.2 shows that adsorption of the metal ions rose steadily from 2 to 6 and then drops again steadily. At pH

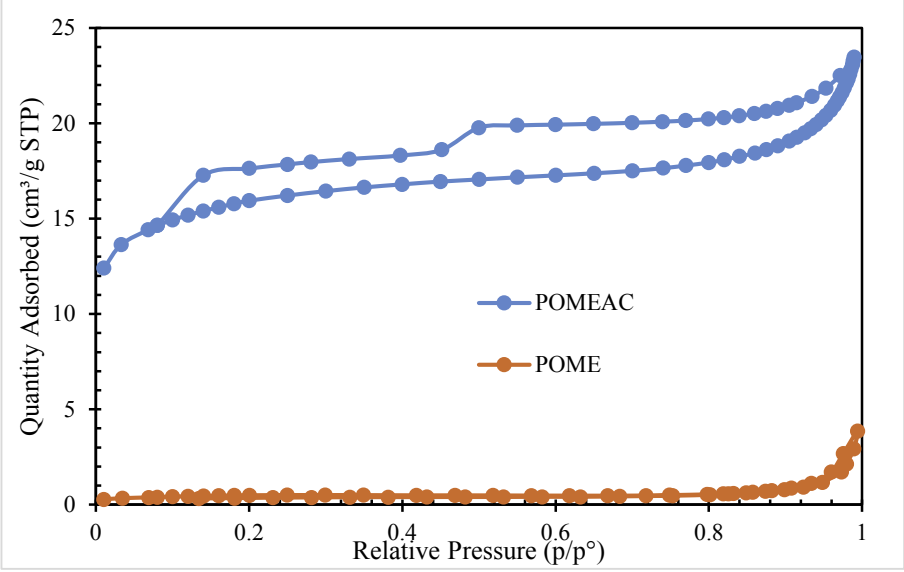

Fig. 2. Nitrogen adsorption-desorption isotherms of POME and POMEAC.

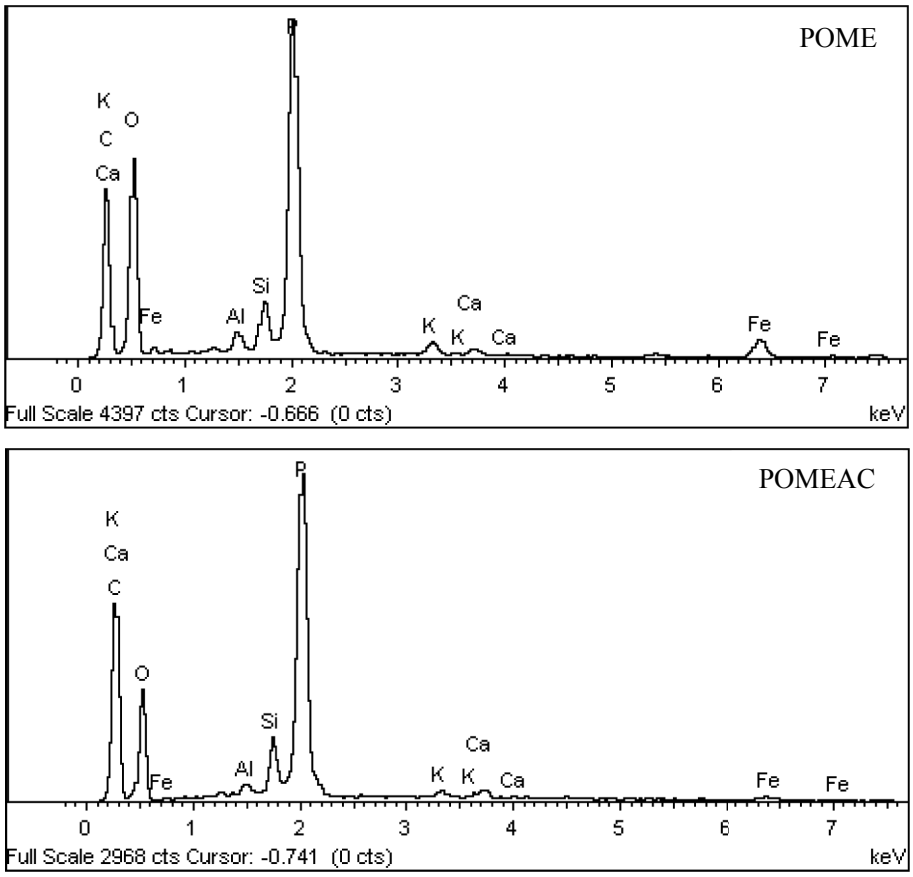

Fig. 3. Energy dispersive X-ray (EDX) analysis of POME and POMEAC.

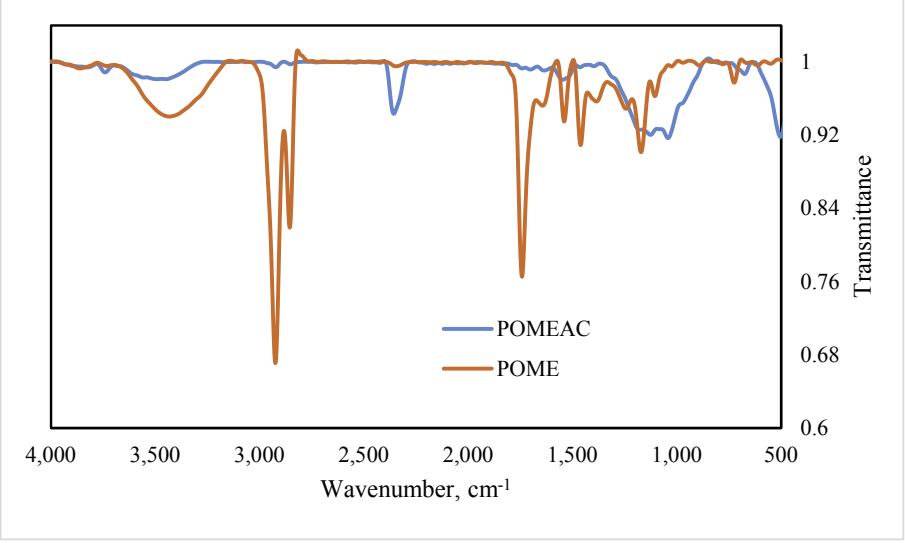

Fig. 4. FTIR analysis of POME and POMEAC.

between 5 and 6, more negatively charged surface are available which no doubt contributed to improved metal ion adsorption. At lower pH values, an adsorbent surface is usually surrounded by hydroxonium ions ($H+$) thereby blocking metal ions from normal binding to adsorbents (Onundi et al., 2010). Equally, at higher pH values of 8 and above, the $OH-$ present in the solution precipitates, thereby blocking available sorption sites and resulting into reduced adsorption (Nguyen et al., 2013). Fig. 7 presents the results of batch adsorption carried out at these varying time. From the figures, it was observed that the sorption level of POMEAC increased progressively as the sorption time increases. The equilibrium time was attained after 50 min for both metal ions. This suggests that all the available sorption sites have been occupied by the cation under investigation. This is similar in trends to what had already been

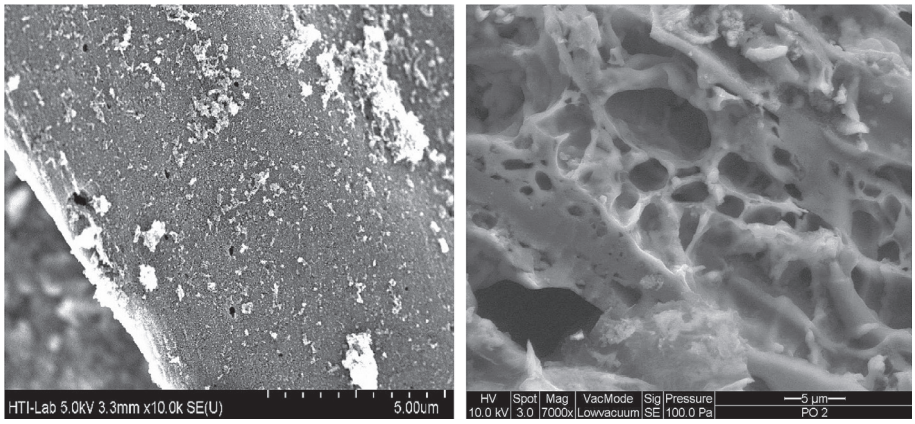

Fig. 5. FESEM images of POME and POMEAC.

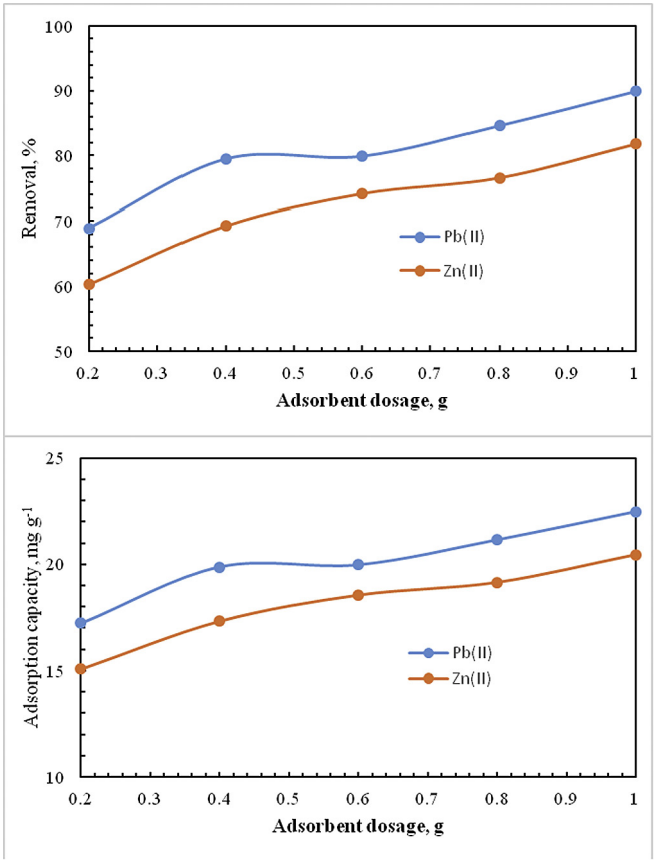

Fig. 6. Effect of adsorbent dosage on (a) percentage metal ion removal, and (b) equilibrium adsorption capacity.

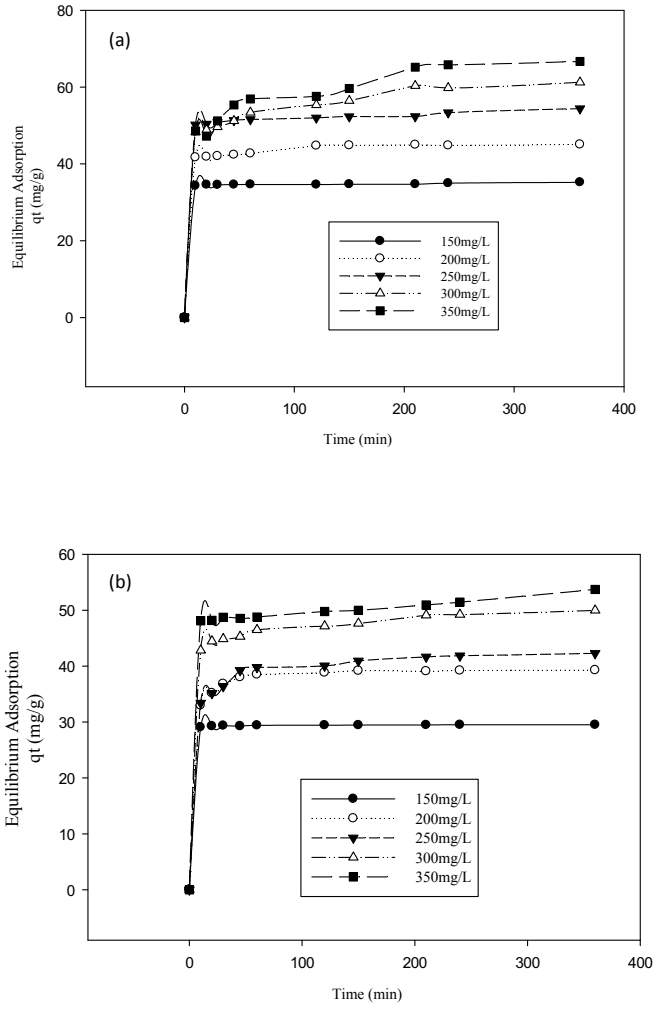

Fig. 7. Effect of initial concentration (a) Pb^{2+} and (b) Zn^{2+} ion and contact time (min): at temperature 30 °C and pH 5.5.

observed by Lupea et al. (2012).

Quite a few kinetic models were used to determine the rate controlling step and study the sorption mechanism of Pb (II) and Zn (II) onto POMEAC. Intra-particle diffusion model was used to compute the rate controlling step, while pseudo first-order, pseudo second-order kinetic (Kumar et al., 2012), and Elovich models were used to compute the rate constant. The prospect of the intra-particle diffusion was utilized as follows (Weber and Morris, 1964):

$$q_t = k_{id} t^{1/2} + C \quad (2)$$

where qt (mg g^{-1}) is the amount of adsorbate adsorbed on the adsorbent at time t, k_{id} (mg g^{-1} $min^{1/2}$) is the intra-particle diffusion rate constant, and C (mg g^{-1}) is the constant, which is proportional to the boundary layer thickness; that is the value of C increases with increase in the boundary layer thickness (Mckay et al., 1980).

The diffusion controlled sorption process is presented by the

Table 2
Kinetic model parameters for the adsorption of Pb(II) onto POMEAC.

C_0 (mg/L)	q_e, exp (mg/g)	Pseudo-first-order			Pseudo-second-order			Elovich model			Intraparticle diffusion		
		q_e, cal (mg/g)	K_1 (g/mg h)	R^2	q_e, cal (mg/g)	K_2 (g/mg h)	R^2	(1/b)ln(ab) (mg/g)	1/b (mg/g)	R^2	K_{id}	C	R^2
150	34.72	0.83	0.0030	0.0006	46.51	0.0008	0.8736	34.70	0.07	0.0073	0.0126	34.53	0.4600
200	44.98	1.87	0.0161	0.8751	71.43	0.0002	0.7701	38.40	1.19	0.9025	0.2612	40.91	0.8737
250	52.30	1.86	0.0048	0.8874	67.57	0.0007	0.9324	47.34	1.05	0.8964	0.2427	49.46	0.9548
300	56.44	3.25	0.0094	0.8373	86.96	0.0003	0.8472	37.29	3.96	0.9443	0.8948	45.43	0.9646
350	62.19	5.85	0.0078	0.9878	116.28	0.0008	0.7625	19.99	14.99	0.9212	3.4284	10.43	0.9638

straight line graph of q_t versus $t^{1/2}$ gives a slope of k_{id} and intercept of C. Tables 2 and 3 gives the values of k_{id} and C for Pb (II) and Zn (II).

If the plot passes through the origin, then intraparticle diffusion remains the only rate-controlling step, else it is not the only rate determining factor due to the effect of boundary layer diffusion on adsorption. For the removal of both Pb(II) and Zn(II) using POMEAC, the linear curves deviated from the origin due to the variation in the diffusion rate in the initial and final stages of the sorption. Since the plots did not pass through origin, then the intraparticle diffusion is not the only factor that determines the rate for the two metal ions.

Elovich model was used to describe sorption on the surface of an adsorbent without product desorption. The model is considered suitable for some chemisorption processes, which involves valence forces via exchange or sharing of between the adsorbate and the adsorbent. The removal rate decreases with time because of the coverage of the active sites (Aharoni and Tompkins, 1970). Elovich model is given by

$$\frac{dq_t}{dt} = a\exp(-bq_t) \tag{3}$$

where a and b are the experimental constants and a is the initial rate as dq_t/dt approaches a and q_t approaches 0.

Given that $q_t = q_t$ at t = t and $q_t = 0$ at t = 0, the integrated form of the above equation is

$$q_t = \left(\frac{1}{b}\right)\ln(t + t_0) - \left(\frac{1}{b}\right)\ln t_0 \tag{4}$$

where $t_0 = 1/ab$. If $t \gg t_0$, the equation can be further simplified as

$$q_t = \left(\frac{1}{b}\right)\ln(ab) + \left(\frac{1}{b}\right)\ln t \tag{5}$$

The intercept and slope of the linear plot of qt vs. ln t gives (1/b) ln(ab) and (1/b). Table 1 shows the parameter values as well as the correlation coefficient (R^2), which shows the uniformity of the predicted values with the experimental data. The model shows good correlation for sorption of both Pb (II) and Zn (II) on POMEAC especially at initial concentration range of 200–350 mg L^{-1} for Pb (II) and 250–300 mg L^{-1} for Zn (II). This indicates that Chemisorption may be the rate-determining step.

Pseudo-first-order kinetic model is given by

$$\frac{1}{q_t} = \frac{k_1}{q_e t} + \frac{1}{q_e} \tag{6}$$

where q_e represents the quantity adsorbed at equilibrium, k_1 (min^{-1}) denotes the pseudo-first-order adsorption rate constant, and q_t symbolizes the quantity absorbed at time t (min), both in mmol g^{-1}. The linear plot of ln $1/q_t$ vs. 1/t gives the value of k_1 and q_e (Table 1).

The pseudo-second-order kinetic model is given by

$$\frac{t}{q_t} = \frac{1}{k_2 q_e^2 t} + \frac{1}{q_e}t \tag{7}$$

where k_2 is the pseudo-second-order adsorption rate constant in g $mmol^{-1}$ min^{-1}, q_t and q_e are the quantity of each heavy metal ion adsorbed at time t (min) and equilibrium, both in mmol g^{-1}. The linear plot of ln t/q_t vs. t gives the value of k_1 and q_t (Tables 2 and 3). The validity of the model was checked using the values of R^2).

The values of q_e experimental and q_e calculated differs appreciably in pseudo-first-order kinetic model, while the values are closer for pseudo-second-order kinetic model at almost all the initial concentrations for both Pb (II) and Zn (II). Further, the R^2 values for pseudo-first-order model were less than that of the pseudo-second-order model for both ions signifying that the pseudo-second-order is better correlated than the pseudo-first-order model. The same kinetic behavior was reported for the adsorption of Pb (II) and Zn (II) onto various adsorbents, such as, activated carbon (Mishra and Patel, 2009); . Maghemite nanotubes (Roy and Bhattacharya, 2012), EDCMS (Ren et al., 2013), MNPs-NH_2 (Tan et al., 2012), tetrasulfide-functionalized silica (Fan et al., 2012), magnetic $Co_{0.6}Fe_2.4O_4$ (Duan et al., 2015), Fe_3O_4-TETA-CMCS (Dabrowski et al., 2004).

3.5. Adsorption isotherm modeling

Figs. 8 and 9 presents the adsorption isotherms of Pb(II) and Zn(II). Isotherms provide the equilibrium relations between the adsorbate concentration on the solid and the liquid phase. The maximum adsorption capacity is obtainable from the isotherms (Ayanda et al., 2013). This provide insight on the adsorbent capacity or the quantity of the adsorbent needed to remove a unit mass of metal ion from aqueous medium under the process conditions.

Table 3
Kinetic model parameters for the adsorption of Zn(II) onto POMEAC.

C_0 (mg/L)	q_e, exp (mg/g)	Pseudo-first-order			Pseudo-second-order			Elovich model			Intraparticle diffusion		
		q_e, cal (mg/g)	K_1 (g/mg h)	R^2	q_e, cal (mg/g)	K_2 (g/mg h)	R^2	(1/b)ln(ab) (mg/g)	1/b (mg/g)	R^2	K_{id}	C	R^2
150	29.46	0.87	0.0147	0.8567	29.50	0.1223	1.0000	28.89	0.11	0.8642	0.0231	29.15	0.7348
200	39.19	1.80	0.0170	0.8652	39.68	0.0086	0.9998	30.65	1.64	0.8332	0.3214	34.51	0.6399
250	43.81	2.77	0.0064	0.9757	42.37	0.0024	0.9979	24.57	2.81	0.9430	0.6432	30.29	0.9855
300	49.63	2.44	0.0071	0.8414	68.49	0.0011	0.5951	36.37	2.58	0.9760	0.5730	41.78	0.9610
350	49.98	2.17	0.0030	0.8085	53.19	0.0036	0.9980	44.38	1.21	0.8579	0.3035	46.60	0.8207

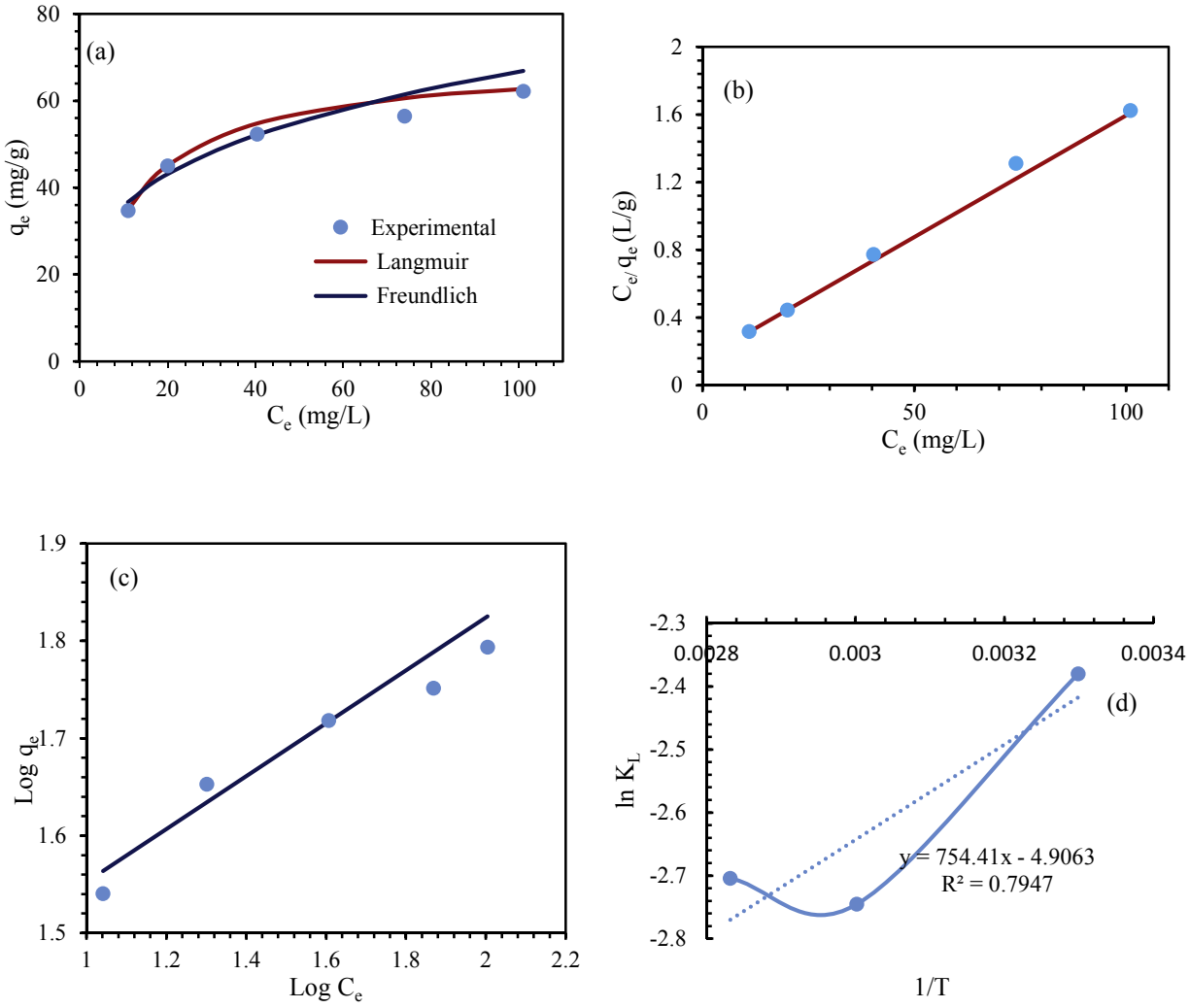

Fig. 8. Adsorption isotherm data for Pb(II) onto POMEAC at 303 K: (a) theoretical and experimental data at pH 5.5, (b) a plot of Ce/qe vs. Ce, (c) linear form of Freundlich, (d) a plot of $\ln K_L$ vs. 1/T using Langmuir model.

Langmuir and Freundlich isotherms are the most commonly used isotherms to describe the solid–liquid adsorption system. The Langmuir isotherms assumes that sorption occurs at a specific homogeneous site on the surface of POMEAC, and that not more than one adsorbate molecule can occupy a site. Langmuir adsorption model is given by

$$\frac{C_e}{q_e} = \frac{1}{k_L q_m} + \frac{C_e}{q_m} \tag{8}$$

where q_e is the quantity of solute adsorbed at equilibrium in mmol g^{-1}, C_e is the equilibrium concentration of the adsorbate in aqueous solution (mmol L^{-1}), q_m (mmol g^{-1}) is the maximum monolayer adsorption capacity, K_L is the Langmuir adsorption constant L $mmol^{-1}$, which indicates the energy of adsorption. The values of K_L and q_m are computed from the linear plot of C_e/q_e vs. C_e. (Figs. 8b and 9b), and the values were displayed in Table 4.

The maximum monolayer sorption capacity (q_m) increases with increase in temperature from 303.15 to 353.15 K (Table 4). Pb (II) exhibits 94.34 mg g^{-1} at 353.15 K and 68.49 mg g^{-1} at 353.15 K for Zn (II) indicating that this system is effective and results are comparable to the previous studies related to heavy metal ions removal.

Weber and Chakravorti (1974) expressed the essential characteristics of Langmuir isotherm by a modeling a dimensionless constant known as the separation factor or equilibrium parameter, R_L, which shows the nature of the adsorption process.

$$R_L = \frac{1}{1 + K_L C_0} \tag{9}$$

where C_0 (mg L^{-1}) is the initial adsorbate quantity and K_L is the Langmuir sorption constant (L mg^{-1}) described above. Adsorption is favorable when the value of R_L is between 0 and 1. The R_L parameter is said to be a more consistent indicator of the adsorption nature. The value of R_L classifies the isotherm to be either favorable ($0 < R_L < 1$), linear ($R_L = 1$), unfavorable ($R_L > 1$) or irreversible ($R_L = 0$). The R_L values for both Pb(II) and Zn(II) (Table 5) show that the adsorption process is favorable by POMEAC. Moreover, the values of the R^2, which determine the uniformity of the predicted values with the experimental data shows that Langmuir model is suitable for both Pb(II) and Zn(II).

Freundlich isotherm is a special case of Langmuir model. It is an empirical model that presents interactions between the adsorbed molecules in a heterogeneous system. The model is applicable to non-ideal adsorption on heterogeneous surfaces and multilayer adsorption (Wang and Qin, 2005), and is given by

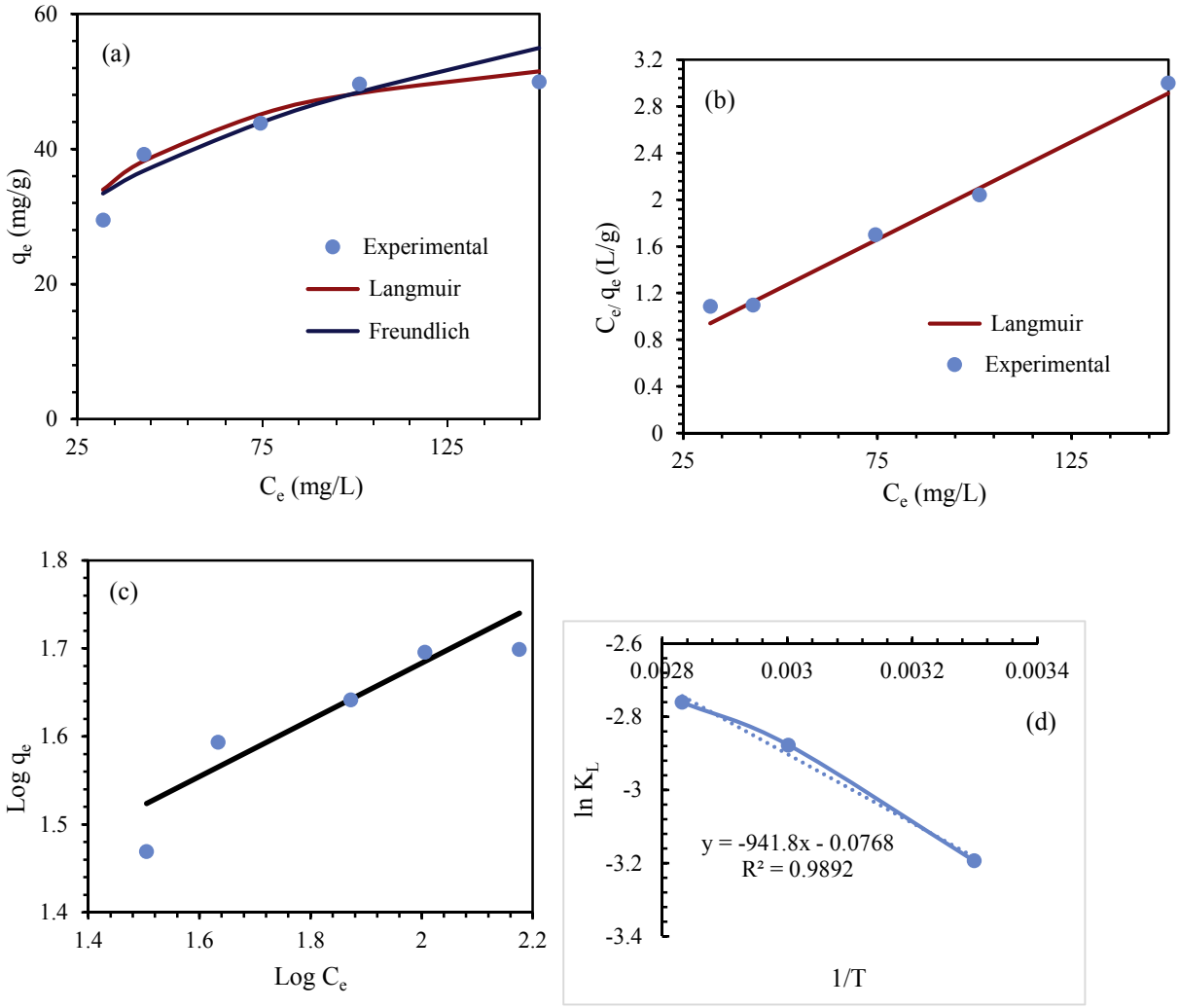

Fig. 9. Adsorption isotherm data for Zn(II) onto POMEAC at 303 K: (a) theoretical and experimental data at pH 5.5, (b) a plot of Ce/qe vs. Ce, (c) linear form of Freundlich, (d) a plot of $\ln K_L$ vs. 1/T using Langmuir model.

Table 4
Langmuir isotherm for sorption of Pb(II) and Zn(II) onto POMEAC at different temperatures.

Temp	Pb(II)			Zn(II)		
	q_m	K_L	R^2	q_m	K_L	R^2
K	(mg/g)	(L/mg)		(mg/g)	(L/mg)	
303.15	69.4444	0.0925	0.9961	59.8802	0.0410	0.9811
333.15	90.0901	0.0642	0.9272	67.5676	0.0563	0.9728
353.15	94.3396	0.0669	0.9519	68.4932	0.0633	0.9686

Table 5
Separation factor, RL values for the Pb(II) and Zn(II) adsorption.

C_0 (mg/L)	Lead	Zinc
	R_L	R_L
150	0.0672	0.1397
200	0.0513	0.1086
250	0.0414	0.0888
300	0.0348	0.0751
350	0.0299	0.0651

$$\ln q_e = \ln k_f + \frac{1}{n} \ln C_e \quad (10)$$

where q_e is the equilibrium concentration of the solute adsorbed on adsorbent (mmol g^{-1}), C_e is the solute equilibrium concentration of the (mmol L^{-1}), K_f is the Freundlich constant, which indicates the adsorption extent in mmol$^{1-1/n}$ $L^{1/n}$ g^{-1}, and n is the heterogeneity factor, which indicates the removal effectiveness. The slope and intercept of ln C_e vs. ln q_e (Figs. 8c and 9c) gives the Values of n and K_f for the metal ions adsorption on POMEAC (Table 6). Since the values of R^2 for both metal ions isotherms are lower than 0.9 for Zn(II), the model cannot adequately give the detail description of the relationship between the quantity of metal ions adsorbed by the POMEAC and its equilibrium concentration in the aqueous medium. For Pb(II), the values of K_f decreases with increase in

Table 6
Freundlich isotherm for sorption of Pb(II) and Zn(II) onto POMEAC at different temperatures.

Temp K	Pb(II)			Zn(II)		
	K_F (mg/g)	n	R^2	K_F (mg/g)	n	R^2
303.15	19.1136	3.6860	0.9294	10.9300	3.1017	0.7828
333.15	15.4808	2.6062	0.9415	12.7764	2.9464	0.7615
353.15	16.0997	2.5536	0.9745	13.3886	2.9412	0.7037

Table 7
Thermodynamic parameters for sorption of Pb(II), and Zn(II).

Temp (K)	Lead			Zinc		
	ΔG°	ΔS°	ΔH°	ΔG°	ΔS°	ΔH°
303.15	5.9987	6.2726	0.0408	8.0480	-7.8301	0.0006
333.15	7.6037			7.9692		
353.15	7.9400			8.1052		

temperature from 303.15 to 333 K indicating that adsorption process is exothermic in nature. However, further increase in temperature to 353.15 K decreases the K_f value. For Zn(II), the values of K_f increases with temperature increase from 303.15 to 353 K indicating that the nature of the adsorption process is endothermic. The values of n for both metal ions fall between 1 and 10 signifying favorable sorption.

The equilibrium observations for Pb(II) shows that both Langmuir and Freundlich model remarkably describe the sorption process. This is inline with the report of Mishra and Patel (2009). Meanwhile, the Langmuir isotherm model best describe Zn(II) removal process, which corroborates the report of Roy and Bhattacharya (2012).

3.6. Thermodynamic analysis

The thermodynamic parameters of the sorption process Gibbs free energy change (ΔG°), the entropy change (ΔS°), and enthalpy change (ΔH°), were obtained from the Langmuir constant (K_L) variation with temperature (T) using the following equations,

$$\Delta G^{\circ} = -RT \ln K_L \tag{11}$$

$$\Delta G^{\circ} = \Delta H^{\circ} - T\Delta S^{\circ} \tag{12}$$

$$\ln K_L = \frac{\Delta S^{\circ}}{R} - \frac{\Delta H^{\circ}}{RT} \tag{13}$$

where R is the universal gas constant (8.314×10^{-3} kJ mol^{-1} K^{-1}). The enthalpy change due to adsorption of Pb^{2+} and Zn^{2+} ions by POMEAC over the temperature range investigated can be obtained from the linear plots of ln K_L against 1/T using the least squares method (Figs. 8d and 9d). The values of ΔH°, ΔS° and ΔG° for sorption of Pb(II) and Zn(II) by POMEAC at a temperatures range of 303.15–353.15 K (Table 7), show that ΔG° is small but increases with increase in temperature for Pb(II), while it show a little decrease with temperature increase from 303.15 to 333.15 K, but further increase to 353.15 K increased the ΔG°. The positive values of ΔG° reveal that the process is less spontaneous and positive values of ΔH° show the need energy input for the process from the surrounding. Both the sorption of Pb(II) and Zn(II) on POMEAC undergo endothermic process. The positive value of ΔS° for Pb(II) removal suggested a more random interaction at the interface of the solid/solution compared to Zn(II) removal with a negative value of ΔS° during the sorption of metal ions on POMEAC. Base on the R^2 value, Langmuir model is more suitable for determination of the thermodynamic parameters of Zn (R2 = 0.989) compared to Pb (R2 = 0.794).

4. Conclusion

An activated carbon was produced from POME and utilized for sorption of Pb(II) and Zn(II) from wastewater over a wide range of adsorbent dosage and metal ion concentrations. The following inferences were reached as the results of this work:

- The activated carbon was characterized by EDX, FTIR and FESEM techniques.
- The adsorption of Pb(II) and Zn(II) increase from 34.72 to 62.19 mg g^{-1} and 29.46–49.98 mg g^{-1} as the initial concentration increases from 150 to 350 mg L^{-1}. Increase in the adsorbent dosage from 0.2 to 1 g resulted in gradual increase in the equilibrium adsorption capacity (mg g^{-1}) of POMEAC from 17.23 to 22.46 fro Pb(II) and 15.08 to 20.45, and increases in the percent removal efficiency.
- Based on R^2 value and difference between the experimental and the calculate values of q_e, pseudo second-order kinetic rather than the pseudo-first-order kinetic model are best fitted for removal of P(II) and Zn(II) from wastewater. In addition, based on the suitability of the Elovich equation for both Pb(II) and Zn(II) we can suggest that the rate determining step for both metal ions is chemisorption. The intraparticle diffusion model for the both Pb(II) and Zn(II) removal with respect to the intercept show greater boundary layer effect. The intraparticle diffusion is not the only rate controlling step.
- The equilibrium observations for Pb(II) shows that both Langmuir and Freundlich model remarkably describe the sorption process. Meanwhile, the Langmuir isotherm model best describe Zn(II) removal process. The maximum monolayer Pb(II) sorption capacity is 94.34 mg g^{-1} at 353.15 K and 68.49 mg g^{-1} at 353.15 K for Zn(II) indicating that this system is effective and results are comparable to the previous studies related to heavy metal ions removal.
- The thermodynamic data show that the removal of Pb(II) and Zn(II) onto POMEAC from wastewater is feasible and endothermic in nature.

Based on the above findings, it is obvious that the synthesized POMEAC is an effective biosorbent for removal of Pb(II) and Zn(II) from wastewater. POMEAC could be used as a biosorbent for other divalent metal ions such as Cd^{2+}, Cu^{2+} and Ni^{2+}.

Acknowledgements

This study was carried out with the aid of a High impact research (HIR) grant (H-21001-F0032) under the University of Malaya.

References

Aharoni, C., Tompkins, F., 1970. Kinetics of adsorption and desorption and the Elovich equation. Adv. Catal. Relat. Subj. 21, 1–49.
Alaba, P.A., Sani, Y.M., Daud, W.M.A.W., 2015. Kaolinite properties and advances for solid acid and basic catalyst synthesis. RSC Adv. 5 (122), 101127–101147.
Alaba, P.A., Sani, Y.M., Mohammed, I.Y., Abakr, Y.A., Daud, W.M.A.W., 2016a. Synthesis and characterization of sulfated hierarchical nanoporous faujasite zeolite for efficient transesterification of shea butter. J. Clean. Prod. 142, 1987–1993. http://dx.doi.org/10.1016/j.jclepro.2016.11.085.
Alaba, P.A., Sani, Y.M., Mohammed, I.Y., Daud, W., Ashri, W.M., 2016b. Insight into catalyst deactivation mechanism and suppression techniques in thermocatalytic deoxygenation of bio-oil over zeolites. Rev. Chem. Eng. 32 (1), 71–91.
Amuda, O., Giwa, A., Bello, I., 2007. Removal of heavy metal from industrial wastewater using modified activated coconut shell carbon. Biochem. Eng. J. 36 (2), 174–181.
Ayanda, O.S., Fatoki, O.S., Adekola, F.A., Ximba, B.J., 2013. Kinetics and equilibrium models for the sorption of tributyltin to nZnO, activated carbon and nZnO/activated carbon composite in artificial seawater. Mar. Pollut. Bull. 72 (1), 222–230.
Baccar, R., Bouzid, J., Feki, M., Montiel, A., 2009. Preparation of activated carbon from Tunisian olive-waste cakes and its application for adsorption of heavy metal ions. J. Hazard. Mater. 162 (2), 1522–1529.
Board, M.P.O., 2003. Oil Palm Fruit Grading Manual. Malaysian Palm Oil Board, Kajang, Malaysia.
Chavalparit, O., 2006. Clean Technology for the Crude Palm Oil Industry in Thailand. Wageneningen University Wageneningen, The Netherlands.
Chigondo, F., Nyamunda, B., Sithole, S., Gwatidzo, L., 2013. Removal of lead (II) and copper (II) ions from aqueous solution by baobab (Adononsia digitata) fruit

shells biomass. IOSRJ. Appl. Chem. 5 (1), 43–50.
Chowdhury, Z.Z., Zain, S.M., Khan, R.A., Islam, M.S., 2012a. Preparation and characterizations of activated carbon from kenaf fiber for equilibrium adsorption studies of copper from wastewater. Korean J. Chem. Eng. 29 (9), 1187–1195.
Chowdhury, Z.Z., Zain, S.M., Khan, R.A., Rafique, R.F., Khalid, K., 2012b. Batch and fixed bed adsorption studies of lead (II) cations from aqueous solutions onto granular activated carbon derived from Mangostana garcinia shell. BioResources 7 (3), 2895–2915.
Chowdhury, Z.Z., Zain, S.M., Khan, R.A., Arami-Niya, A., Khalid, K., 2012c. Process variables optimization for preparation and characterization of novel adsorbent from lignocellulosic waste. BioResources 7 (3), 3732–3754.
Dabrowski, A., Hubicki, Z., Podkościelny, P., Robens, E., 2004. Selective removal of the heavy metal ions from waters and industrial wastewaters by ion-exchange method. Chemosphere 56 (2), 91–106.
Duan, S., Tang, R., Xue, Z., Zhang, X., Zhao, Y., Zhang, W., Zhang, J., Wang, B., Zeng, S., Sun, D., 2015. Effective removal of Pb (II) using magnetic Co 0.6 Fe 2.4 O 4 micro-particles as the adsorbent: synthesis and study on the kinetic and thermodynamic behaviors for its adsorption. Colloids Surf. A: Physicochem. Eng. Aspects 469, 211–223.
Ekebafe, L., Ekebafe, M., Erhuaga, G., Oboigba, F., 2012. Effect of reaction conditions on the uptake of selected heavy metals from aqueous media using composite from renewable materials. Am. J. Polym. Sci. 2 (4), 67–72.
Fan, H.-T., Wu, J.-B., Fan, X.-L., Zhang, D.-S., Su, Z.-J., Yan, F., Sun, T., 2012. Removal of cadmium (II) and lead (II) from aqueous solution using sulfur-functionalized silica prepared by hydrothermal-assisted grafting method. Chem. Eng. J. 198, 355–363.
Foo, K., Hameed, B., 2011. Preparation of oil palm (Elaeis) empty fruit bunch activated carbon by microwave-assisted KOH activation for the adsorption of methylene blue. Desalination 275 (1), 302–305.
Gratuito, M.K.B., Panyathanmaporn, T., Chumnanklang, R.-A., Sirinuntawittaya, N., Dutta, A., 2008. Production of activated carbon from coconut shell: optimization using response surface methodology. Bioresour. Technol. 99 (11), 4887–4895.
Habib, M., Yusoff, F., Phang, S., Ang, K., Mohamed, S., 1997. Nutritional values of chironomid larvae grown in palm oil mill effluent and algal culture. Aquaculture 158 (1), 95–105.
Hameed, B., Ahmad, A., Latiff, K., 2007. Adsorption of basic dye (methylene blue) onto activated carbon prepared from rattan sawdust. Dyes Pigments 75 (1), 143–149.
Igwe, J., Onyegbado, C., 2007. A review of palm oil mill effluent (POME) water treatment. Glob. J. Environ. Res. 1 (2), 54–62.
Kumar, N.S., Woo, H.-S., Min, K., 2012. Equilibrium and kinetic studies on biosorption of 2, 4, 6-trichlorophenol from aqueous solutions by Acacia leucocephala bark. Colloids Surf. B: Biointerfaces 94, 125–132.
Lupea, M., Bulgariu, L., Macoveanu, M., 2012. Biosorption of Cd(II) from aqueous solutions on marine algae biomass. Environ. Eng. Manag. J. 11 (3), 607–615.
Mckay, G., Otterburn, M., Sweeney, A., 1980. The removal of colour from effluent using various adsorbents—III. Silica: rate processes. Water Res. 14 (1), 15–20.
Mi, T., Chen, L., Xin, S.-z., Yu, X.-m., 2015. Activated carbon from the Chinese herbal medicine waste by H3PO4 activation. J. Nanomater. 2015.
Mishra, P., Patel, R., 2009. Removal of lead and zinc ions from water by low cost adsorbents. J. Hazard. Mater. 168 (1), 319–325.
Nacu, G., Bulgariu, D., Cristina Popescu, M., Harja, M., Toader Juravle, D., Bulgariu, L., 2015. Removal of Zn (II) ions from aqueous media on thermal activated sawdust. Desalin. Water Treat. 1–12.
Naje, S.A., Chelliapan, Shreeshivadasan, Zakaria, Zuriati, Ajeel, Mohammed A., Alaba, P.A., 2016. A Review of Electrocoagulation Technology for the Treatment of Textile Wastewater. http://dx.doi.org/10.1515/revce-2016-0019.
Nguyen, T., Ngo, H., Guo, W., Zhang, J., Liang, S., Yue, Q., Li, Q., Nguyen, T., 2013. Applicability of agricultural waste and by-products for adsorptive removal of heavy metals from wastewater. Bioresour. Technol. 148, 574–585.
Onundi, Y.B., Mamun, A., Al Khatib, M., Ahmed, Y.M., 2010. Adsorption of copper, nickel and lead ions from synthetic semiconductor industrial wastewater by palm shell activated carbon. Int. J. Environ. Sci. Technol. 7 (4), 751–758.
Oswal, N., Sarma, P., Zinjarde, S., Pant, A., 2002. Palm oil mill effluent treatment by a tropical marine yeast. Bioresour. Technol. 85 (1), 35–37.
Phang, S.-M., 1990. Algal production from agro-industrial and agricultural wastes in Malaysia. Ambio 415–418.
Phang, S.-M., Kim-Chong, O., 1988. Algal biomass production in digested palm oil mill effluent. Biol. Wastes 25 (3), 177–191.
Ren, Y., Abbood, H.A., He, F., Peng, H., Huang, K., 2013. Magnetic EDTA-modified chitosan/SiO 2/Fe 3 O 4 adsorbent: preparation, characterization, and application in heavy metal adsorption. Chem. Eng. J. 226, 300–311.
Roy, A., Bhattacharya, J., 2012. Removal of Cu (II), Zn (II) and Pb (II) from water using microwave-assisted synthesized maghemite nanotubes. Chem. Eng. J. 211, 493–500.
Sani, Y.M., Raji-Yahya, A.O., Alaba, P.A., Aziz, A.R.A., Daud, W.M.A.W., 2015. Palm Frond and Spikelet as environmentally benign alternative solid acid catalysts for biodiesel production. BioResources 10 (2), 3393–3408.
Sing, K.S., 1985. Reporting physisorption data for gas/solid systems with special reference to the determination of surface area and porosity (Recommendations 1984). Pure Appl. Chem. 57 (4), 603–619.
Tan, Y., Chen, M., Hao, Y., 2012. High efficient removal of Pb (II) by amino-functionalized Fe 3 O 4 magnetic nano-particles. Chem. Eng. J. 191, 104–111.
Tseng, R.-L., 2007. Physical and chemical properties and adsorption type of activated carbon prepared from plum kernels by NaOH activation. J. Hazard. Mater. 147 (3), 1020–1027.
Wang, X.-s., Qin, Y., 2005. Equilibrium sorption isotherms for of Cu 2+ on rice bran. Process Biochem. 40 (2), 677–680.
Weber, T.W., Chakravorti, R.K., 1974. Pore and solid diffusion models for fixed-bed adsorbers. AIChE J. 20 (2), 228–238.
Weber, W., Morris, J.C., 1964. Equilibria and capacities for adsorption on carbon. Sanit. Eng. Div. 90, 79–91.